Yide Gao, Peter Glarborg, and Paul Marshall*

The Reaction Kinetics of Amino Radicals with Sulfur Dioxide

DOI 10.1515/zpch-2015-0637
Received April 29, 2015; accepted June 18, 2015

Abstract: Application of the laser photolysis–laser-induced fluorescence method to the reaction $NH_2 + SO_2$ in argon bath gas yields pressure-dependent, third-order kinetics which may be summarized as $k = (1.49 \pm 0.15) \times 10^{-31} (T/298\ \mathrm{K})^{-0.83}\ \mathrm{cm^6\ molecule^{-2}\ s^{-1}}$ over 292–555 K, where the uncertainty is the 95% confidence interval and includes possible systematic errors. The quenching of vibrationally excited NH_2 is consistent with a high-pressure limit for $NH_2 + SO_2$ of $(1.62 \pm 0.25) \times 10^{-11}\ \mathrm{cm^3\ molecule^{-1}\ s^{-1}}$ over the temperature range 295–505 K, where again the 95% confidence interval is shown. *Ab initio* analysis yields a $H_2N–SO_2$ dissociation enthalpy of 73.5 kJ mol^{-1}, and comparison with RRKM theory and the exponential down model for energy transfer yields $\langle \Delta E \rangle_{\mathrm{down}} = 350\ \mathrm{cm^{-1}}$ for Ar at room temperature.

Keywords: Reaction Kinetics, NH_2, SO_2, Combustion, RRKM.

Dedicated to Prof. Dr. Dr. h.c. mult. Jürgen Troe on the occasion of his 75th birthday

1 Introduction

The interactions between nitrogen and sulfur chemistry in combustion is a field with major uncertainty [1], as it was thirty years ago [2]. Kinetic modeling calcula-

***Corresponding author: Paul Marshall,** Department of Chemistry and Center for Advanced Scientific Computing and Modeling (CASCaM), University of North Texas, 1155 Union Circle #305070, Denton, Texas 76203–5017, United States, e-mail: marshall@unt.edu
Yide Gao: Department of Chemistry and Center for Advanced Scientific Computing and Modeling (CASCaM), University of North Texas, 1155 Union Circle #305070, Denton, Texas 76203–5017, United States; and present address: PPG Industries, 3333 N Interstate 35, Gainesville, Texas 76240, United States
Peter Glarborg: Department of Chemical and Biochemical Engineering, Technical University of Denmark, DK-2800 Kgs. Lyngby, Denmark

tions on the effects of sulfur species on nitrogen conversion to nitrogen oxides are qualitative at best. Premixed flame experiments [3–7] indicate that the NO yield is the result of a complex competition between S/N mechanisms that promote NO formation, inhibit NO formation, and reduce NO already formed, but details of the interactions remain unclear.

Key steps in the sulfur/nitrogen interactions include reaction of amino radicals with sulfur species, and the dominant form is sulfur dioxide. During combustion, fuel-bound nitrogen is mostly converted through the radical species N, NH and NH_2 [8]. The presence of SO_2 affects the oxidation selectivity towards the products NO and N_2 [1]. Also, the selective non-catalytic reduction of NO (SNCR) by NH_3 is sensitive towards the concentration of SO_2 [9–12], which is in part due to the influence of SO_2 on the general pool of radicals such as OH, H and O, but $NH_x + SO_2$ reactions may also contribute.

The reaction of NH_2 with SO_2 has been studied one time previously, by Ioffe et al. [13], who observed a pressure dependence which suggests the mechanism is adduct formation

$$NH_2 + SO_2 + M \rightarrow NH_2SO_2 + M \quad (1)$$

This is analogous to OH addition to SO_2 [14]:

$$OH + SO_2 + M \rightarrow HOSO_2 + M \quad (2)$$

which in a second step can lead to SO_3 formation by H-atom abstraction from $HOSO_2$ by O_2 [15]. In light of the impact of sulfur on nitrogen chemistry in flames, the analogous abstraction from NH_2SO_2 to yield $HNSO_2$ is of interest. The latter molecule is isoelectronic with SO_3. We speculate that if it dissociates to NH + SO_2, then reaction (1) initiates a cycle where SO_2 catalyzes $NH_2 + O_2 \rightarrow$ NH + HO_2, a process which is extremely slow as a direct step [16]. In the present work we conduct new experiments on reaction (1) and argue for a modification of the presently accepted kinetics, and show that the results are consistent with RRKM analysis based on an *ab initio* potential energy surface. We also make predictions of the thermochemistry of $HNSO_2$.

2 Experimental method

Ammonia (MG Industries, 99.99%) and sulfur dioxide (MG Industries, 99.8%) were purified by repeated trapping at 77 K, degassing and warming. Argon ((99.995%, Air Liquide and Big Three) was used directly from the cylinder. We applied the laser photolysis–laser-induced fluorescence (LP-LIF) technique to reaction (1). Details of the stainless steel reaction cell and its use in NH_2 chemistry

have been provided previously [17, 18]. Briefly, dilute mixtures of NH_3 and SO_2 were prepared in a large excess of Ar bath gas. NH_2 is formed by 193 pulsed excimer laser photolysis of the NH_3 precursor, and monitored as a function of time t by LIF at 570.3 nm, which corresponds to excitation of the $A\,^2A_1$ state from ground state $X\,^2B_1$ NH_2. In a few experiments LIF at 531.8 nm was used to follow the kinetics of vibrationally excited (0,1,0) NH_2 [17]. Low photolysis pulse energies F were employed to minimize photolysis of SO_2.

Following the pulsed generation of NH_2, the LIF signal I_f was captured in a boxcar integrator (Stanford Research Systems SR250) and observed to follow an exponential decay with a decay constant k_{ps1} back to a constant background B arising from scattered light from the excitation beam:

$$I_f = A \exp(-k_{ps1} t) + B \tag{3}$$

B does not change with time and was checked carefully by measurements before the probe beam was triggered, and by measurements without the photolysis beam or in the absence of photolytic precursor. An example decay is shown in Figure 1, and is interpreted in terms of the scheme

$$NH_2 + SO_2 \xrightarrow{k_1} \text{products} \tag{4}$$

$$NH_2 \xrightarrow{k'} \text{loss} \tag{5}$$

k' is the effectively first-order loss rate of NH_2 via processes which do not depend on $[SO_2]$, such as diffusion out of the reaction zone that is defined by the intersection of the photolysis and probe beams. The expected rate equation is

$$d[NH_2]/dt = -k_1[NH_2][SO_2] - k'[NH_2] \tag{6}$$

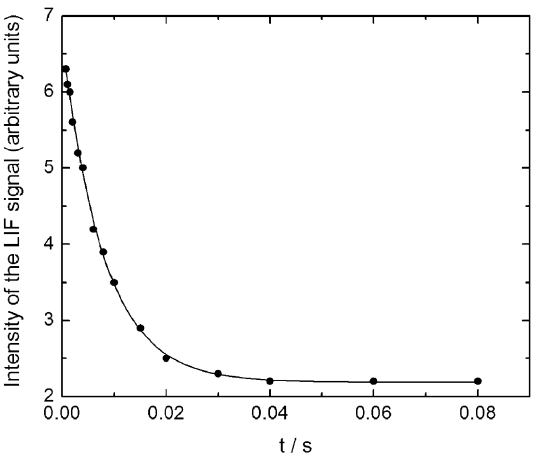

Figure 1: Integrated LIF signal excited at 570.3 nm (0.3 mJ energy) vs. time delay after 193 nm photolysis laser pulse (0.5 mJ), at 412 K, 15 mbar total pressure and $[SO_2] = 1.4 \times 10^{15}$ molecule cm^{-3}. The curve is an exponential fit (see text).

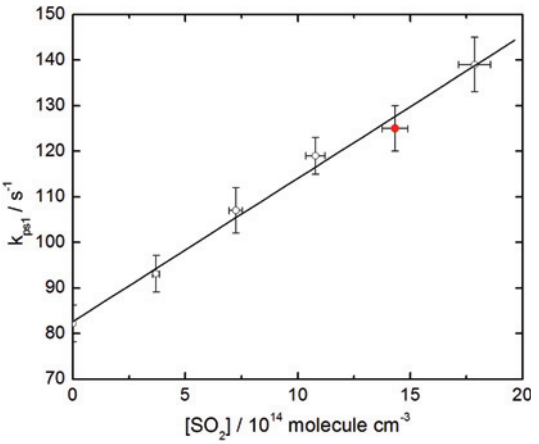

Figure 2: Variation of the pseudo-first-order rate coefficient k_{ps1} for the removal of ground-state NH_2 as a function of the concentration of SO_2 at $T = 412$ K and $p = 15$ mbar. The filled symbol corresponds to the decay shown in Figure 1.

Under the pseudo-first-order condition we employ, $[SO_2] \gg [NH_2]$, $[SO_2]$ is effectively constant so we may write

$$d[NH_2]/dt = -k_{ps1}[NH_2] \tag{7}$$

The pseudo-first-order rate constant k_{ps1} is obtained from non-linear least-squares fitting of I_f to the form of Equation (3). The effective second-order rate constant k_1 and its statistical uncertainty is obtained from a plot of k_{ps1} vs $[SO_2]$, with 6 different values of $[SO_2]$ from 0 to $[SO_2]_{max}$, as shown in Figure 2. The intercept corresponds to k'.

3 Results

Table 1 lists 25 determinations of k_1. These are plotted as a function of [Ar] in Figure 3. It may be seen that there is linear dependence, and the slopes at each temperature define third-order rate constants $k_{1,0}$ when the effective second-order rate constant is

$$k_1 = k_{1,0}[Ar] \tag{8}$$

The $k_{1,0}$ data over 292–555 K are listed in Table 2, from linear plots constrained to pass through the origin, or, for temperatures where there is only a single measurement, from $k_1/[Ar]$. Purely statistical uncertainties are also summarized in Table 2. Figure 3 shows that results with different initial radical concentrations, controlled by the photolysis energy F and the concentrations of NH_3 and SO_2, lie on the same trends. Table 2 lists these concentrations as well as the initial

Table 1: Summary of measurements of the effective second-order rate constant k_1 for SO_2 reaction with NH_2 in its ground and a vibrationally-excited (0,1,0) state.

T, K	τ_{res}, s	F^a, mJ	E^b, mJ	P, mbar	$[SO_2]_{max}$, 10^{15} molecule cm^{-3}	$[O]_{0,max}$, 10^{12} molecule cm^{-3}	[Ar], 10^{17} molecule cm^{-3}	$[NH_3]$, 10^{15} molecule cm^{-3}	$[NH_2]_0$, 10^{12} molecule cm^{-3}	$k_1 \pm \sigma$, 10^{-14} cm^{-3} molecule^{-1} s^{-1}
292	0.9	0.2	0.3	11	0.77 ± 0.03	1.11	2.74	6.40	6.13	3.86 ± 0.25
292	0.8	0.4	0.6	12	3.27 ± 0.13	9.33	2.86	1.18	2.29	4.06 ± 0.11
292	1.0	0.4	0.5	24	2.72 ± 0.11	7.78	5.98	1.23	2.39	8.45 ± 0.51
292	0.8	0.4	0.2	11	2.77 ± 0.11	7.92	2.81	1.11	2.15	4.60 ± 0.29
292	0.8	0.8	0.3	12	1.38 ± 0.06	7.93	2.86	1.10	4.27	4.35 ± 0.31
292	1.8	0.3	0.5	21	2.45 ± 0.10	5.26	5.28	1.17	1.70	7.36 ± 0.49
292	0.9	0.4	0.5	9	2.10 ± 0.08	6.02	2.09	1.03	2.00	3.65 ± 0.21
292	0.7	0.4	0.5	14	1.72 ± 0.07	4.94	3.36	1.05	2.04	5.60 ± 0.34
351	0.9	0.4	0.3	15	1.68 ± 0.07	4.82	3.15	1.06	2.06	4.75 ± 0.25
407	0.6	0.4	0.5	9	2.03 ± 0.08	5.82	1.60	1.13	2.19	1.99 ± 0.12
410	0.8	0.4	0.5	17	1.59 ± 0.06	4.57	2.97	1.13	2.19	2.98 ± 0.17
411	0.7	0.8	0.3	14	1.29 ± 0.05	7.42	2.41	0.92	3.57	2.90 ± 0.16
412	0.7	0.3	0.3	15	1.38 ± 0.06	2.97	2.62	1.29	1.88	3.13 ± 0.15
412	0.7	0.5	0.3	15	1.79 ± 0.07	6.42	2.62	1.29	3.13	3.20 ± 0.19
412	0.7	0.5	0.7	15	1.45 ± 0.06	5.21	2.65	1.31	3.18	3.22 ± 0.17
413	1.2	0.5	0.5	25	1.11 ± 0.04	3.99	4.41	1.36	3.30	4.31 ± 0.25
413	0.7	0.5	0.5	10	1.74 ± 0.07	6.24	1.74	1.11	2.69	2.10 ± 0.13
478	0.6	0.5	0.3	16	1.18 ± 0.05	4.24	2.43	1.01	2.45	2.69 ± 0.19
527	0.5	0.4	0.5	13	1.00 ± 0.04	2.88	1.82	1.15	2.23	2.01 ± 0.13
528	0.6	0.5	0.5	11	1.66 ± 0.07	5.96	1.43	1.27	3.08	1.29 ± 0.08
528	0.5	0.2	0.3	15	0.97 ± 0.04	1.40	2.05	1.24	1.20	2.36 ± 0.13
529	0.5	0.3	0.5	22	1.10 ± 0.04	2.37	3.03	1.19	1.73	3.21 ± 0.19
554	0.5	0.5	0.5	13	1.30 ± 0.05	4.67	1.66	1.34	3.25	1.01 ± 0.05
555	0.4	0.5	0.4	13	1.05 ± 0.04	3.78	1.66	1.28	3.10	1.45 ± 0.09
555	0.5	0.4	0.4	10	1.92 ± 0.08	5.51	1.30	1.18	2.29	1.08 ± 0.06

radical concentrations based on the absorption cross sections at 193 nm [19, 20] and the assumption that the photon yields for H + NH_2 and O + SO_2 are unity. The lack of variation of k_1 with radical concentration is an indication that secondary chemistry, including for example fast consumption of NH_2 by O atoms from SO_2 photolysis, is not significant and that reaction (1) has been successfully isolated from interfering chemistry. The experimental $k_{1,0}$ data are plotted

Table 1: Continued.

T, K	τ_{res}, s	F^a, mJ	E^b, mJ	P, mbar	$[SO_2]_{max}$, 10^{15} molecule cm^{-3}	$[O]_{0,max}$, 10^{12} molecule cm^{-3}	[Ar], 10^{17} molecule cm^{-3}	$[NH_3]$, 10^{15} molecule cm^{-3}	$[NH_2]_0$, 10^{12} molecule cm^{-3}	$k_1 \pm \sigma$, 10^{-14} cm^{-3} molecule^{-1} s^{-1}
295	0.8	0.4	0.6	12	0.19 ± 0.01			0.97		1750 ± 250[c]
295	0.8	0.8	0.6	12	0.64 ± 0.03			0.54		1530 ± 190[c]
295	0.8	0.4	1.2	12	0.65 ± 0.03			0.63		1650 ± 210[c]
352	0.7	0.4	0.7	12	0.52 ± 0.02			0.65		1590 ± 170[c]
412	0.6	0.4	0.6	12	0.62 ± 0.02			1.06		1710 ± 220[c]
504	0.5	0.8	0.6	12	0.57 ± 0.02			0.54		1480 ± 240[c]
505	0.5	0.4	0.6	12	0.50 ± 0.02			0.85		1650 ± 160[c]

[a] Pulse energy for 193 nm photolysis of NH_3.
[b] Pulse energy of dye laser used to excite LIF from NH_2.
[c] Removal rate constant for vibrationally-excited NH_2.

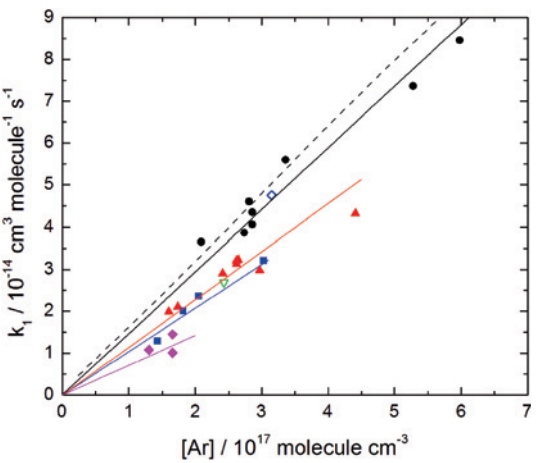

Figure 3: Dependence of effective second-order $NH_2 + SO_2$ rate constants on Ar density. Solid circles, 292 K; open diamond, 351 K; solid triangles, 411 K; open triangle, 478 K; solid squares, 512 K; solid diamonds, 555 K. The solid lines are linear fits through the origin. The dashed line is an RRKM calculation for 292 K (see text).

on Figure 4 and may be summarized by the expression $(1.49 \pm 0.15) \times 10^{-31} (T/298\ \mathrm{K})^{-0.83}$ cm^6 molecule^{-2} s^{-1} over 292–555 K. The uncertainty shown is the 95% confidence interval which also includes an allowance for possible systematic errors.

Table 1 also lists the results of 7 experiments where the bimolecular removal rate constant of vibrationally excited NH_2 was determined. No significant trend with temperature is noted and these results may be summarized as $(1.62 \pm 0.25) \times 10^{-11}$ cm^3 molecule^{-1} s^{-1} over the temperature range 295–505 K, where the uncertainty is the 95% confidence interval.

Table 2: Low-pressure limit rate constant $k_{1,0}$ measured for $NH_2 + SO_2 + Ar$.

T/K	$k_{1,0}/10^{-31}$ cm^6 molecule^{-2} s^{-1} $\pm 2\sigma$
292	1.48 ± 0.05
351	1.51 ± 0.16
411	1.14 ± 0.05
478	1.11 ± 0.16
528	1.04 ± 0.06
555	0.71 ± 0.10

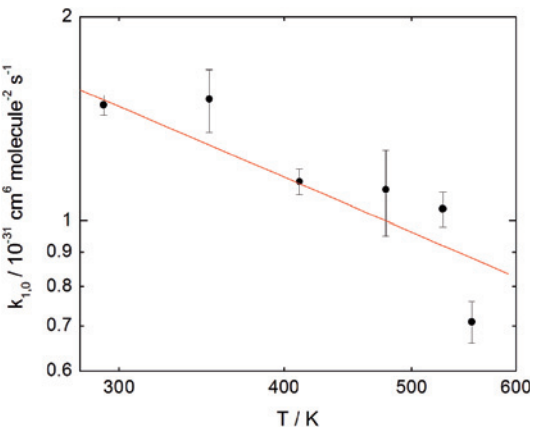

Figure 4: Dependence of the low-pressure limit $k_{1,0}$ for $NH_2 + SO_2 + Ar$ on temperature (log-log plot).

4 Discussion

Our observed $k_{1,0}$ may be interpreted as the low-pressure limiting behavior of the energy transfer mechanism:

$$NH_2 + SO_2 \xrightarrow{k_a} NH_2SO_2^* \quad (9)$$

$$NH_2SO_2^* \xrightarrow{k_{-a}} NH_2 + SO_2 \quad (10)$$

$$NH_2SO_2^* + Ar \xrightarrow{k_b} NH_2SO_2 + Ar \quad (11)$$

Reaction (9) is the initial capture of NH_2 by SO_2 to yield a vibrationally excited intermediate, denoted by *. There is competition between redissociation of this excited adduct (step 10) and collisional stabilization via energy transfer to the Ar bath gas (step 11). At the low-pressure limit $[Ar] \rightarrow 0$, step 11 is rate limiting and

with $[NH_2SO_2{}^*]$ in steady state, we may write

$$d[NH_2]/dt = -k_b(k_a/k_{-a})[Ar][NH_2][SO_2] = -k_{1,0}[Ar][NH_2][SO_2] \quad (12)$$

At the high-pressure limit $[Ar] \rightarrow \infty$, step 9 becomes rate limiting and

$$d[NH_2]/dt = -k_a[NH_2][SO_2] = -k_{1,\infty}[NH_2][SO_2] \quad (13)$$

The slightly negative temperature dependence of $k_{1,0}$ is consistent with expectations for an addition reaction with no barrier, and where the efficiency of collisional transfer to the bath gas decreases with increasing temperature. Luther and Troe have noted that third-order addition rate constants may often be expressed in the form $A\,T^n$. The particular dependence of reaction (1), proportional to $T^{-0.83}$, is in line with other reactions [21]. The magnitude of $k_{1,0}$ is similar to that determined for the analogous reaction (2), and there is accord at room temperature with $k_{2,0}$ (M = Ar) to within 10% [22].

We have explored the potential energy surface for reaction (1) using the CBS-QB3 level of theory as implemented in the Gaussian09 program suite [23]. This is a composite method where geometries and frequencies are obtained with B3LYP/6-311G(2d,d,p) density functional theory, followed by a series of single-point calculations to yield an energy that approximates the coupled-cluster CCSD(T) result with an infinite basis set [24]. Relative enthalpies at 0 K (which include zero-point vibrational energy terms) are drawn in Figure 4. An unfavorable path is attack of NH_2 at an O atom of SO_2, while attack at the S atom can proceed with no barrier. Two structures of NH_2SO_2 are characterized and displayed in Figure 5. The structure denoted IM1 has the N–H bonds staggered with respect to the S–O bonds, and is about 8 kJ mol^{-1} more stable than an alternative geometry where the N–H and S–O bonds are eclipsed. The conformers may isomerize via torsion about the S–N bond. The barrier to this interconversion is much less than the energy available to the newly formed adducts, so we expect these two isomers to be formed in equilibrium, and in the RRKM treatment below this interconversion was treated as a hindered rotation.

We then focused on the reactants and adduct conformers more rigorously, using methods implemented in the Molpro program suite [25]. The geometry and vibrational frequencies were refined with spin-unrestricted CCSD(T) theory with spin-restricted wavefunctions using the aug-cc-pV(T+d)Z basis set, followed by a single-point CCSD(T)/aug-cc-pV(Q+d)Z and CCSD(T)/aug-cc-pV(5+d)Z calculations, to extrapolate the energy to the infinite basis set limit. This energy was corrected for several additional effects. The pwVTZ basis set was used to quantify the influence of scalar relativity as the sum of mass-velocity and Darwin terms at the CCSD level, and the same basis set was used to correct for core-valence

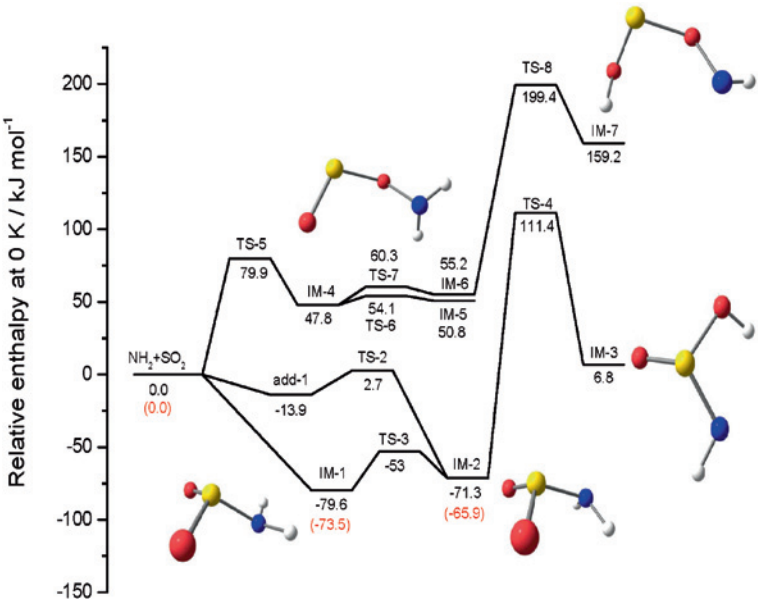

Figure 5: Computed potential energy diagram for $NH_2 + SO_2$ showing relative 0 K enthalpies derived via the CBS-QB3 method. CCSDT(Q)/CBS data shown in parentheses (see text). Structures for IM-5 and IM-6, rotational conformers of IM-4, have been omitted for clarity.

electron correlation at the CCSD(T) level. A term for zero-point vibrational energy was estimated by scaling the harmonic frequencies by a factor of 0.95. Finally a correction for higher level electron correlation was defined as the difference between CCSD(T) and CCSDT(Q) energies with the cc-pVDZ basis set. The results of the calculations are summarized in the supplementary material.

An important piece of information from this *ab initio* work is the $H_2N–SO_2$ bond dissociation enthalpy at 0 K of 73.5 kJ mol^{-1} for the more stable, staggered, isomer. This is about 40 kJ mol^{-1} less strongly bound than $HO–SO_2$. We employ our computed bond strength, along with the CCSD(T) moments of inertia and frequencies, to evaluate a theoretical $k_{1,0}$ via RRKM theory, as implemented within the MultiWell program [26]. There is one adjustable parameter in these kinetic calculations, the average energy transferred from the excited adduct per deactivating collision with Ar bath gas atoms, $\langle \Delta E \rangle_{down}$. Because [Ar] is two orders of magnitude larger than [NH_3] in our work, the role of stabilizing collisions with NH_3 is negligible. Figure 3 shows the good agreement with experiment obtained with the choice of $\langle \Delta E \rangle_{down} = 350$ cm^{-1} and the exponential model for energy transfer. This value of $\langle \Delta E \rangle_{down}$ corresponds [27] to an overall average energy transferred in all up and down transitions $\langle \Delta E \rangle$ of about −2.4 kJ mol^{-1} at 298 K, and

a collisional efficiency $\beta_c = 0.4$, which are typical for unimolecular reactions in Ar bath gas as summarized by Troe [28]. Thus our observations at the low-pressure limit may be rationalized in terms of the PES.

Determination of $k_{1,\infty}$ requires measurements at higher pressures than the 9–25 mbar range we used. In fact, via RRKM theory we estimate fall-off effects to become important above ~ 10 bar at room temperature. However, [Ar] is limited in our LIF experiments because high densities of Ar quench the fluorescence of NH_2. Inspection of Figure 4 indicates no significant falloff behavior with k_1 up to $\sim 10^{-13}$ cm^3 molecule^{-1} s^{-1}, so $k_{1,\infty}$ must be at least equal to this and is probably greater than 10^{-12} cm^3 molecule^{-1} s^{-1}.

For a more quantitative evaluation, we estimate $k_{1,\infty}$ via the removal rate of vibrationally excited NH_2^*. As proposed by Smith and coworkers [29], randomization of energy within the initial adduct means that even if it redissociates rapidly, the rate of loss of NH_2^* might be similar to the ground state NH_2 capture rate. In the case of reaction (2), Blitz et al. made detailed RRKM arguments as to why intramolecular vibrational energy redistribution (IVR) is likely to be complete [14] in $HOSO_2$, and so this seems plausible for H_2NSO_2 also. On this basis and using the data in Table 1, we estimate $k_{1,\infty} = 1.6 \times 10^{-11}$ cm^3 molecule^{-1} s^{-1}. This lies between the hard-sphere collision rate of $\sim 10^{-10}$ cm^3 molecule^{-1} s^{-1} and the high-pressure limit observed for reaction (2), of around 2×10^{-12} cm^3 molecule^{-1} s^{-1}. It should be noted that notwithstanding the analysis of the $HOSO_2$ analog [14], there can be situations where excess vibrational energy in an initially excited reactant can be lost collisionally via non-reactive relaxation instead [30], which would mean the estimate of $k_{1,\infty}$ is too high. Our value is therefore strictly an upper limit.

Our results for reaction (1) may be contrasted with the only prior study, by Ioffe et al. [13]. They employed intra-cavity laser absorption by NH_2. They obtained $k_{1,0}$ at 298 K for M = N_2 and NH_3 of $(3.2 \pm 0.6) \times 10^{-32}$ cm^6 molecule^{-2} s^{-1} and $(2.1 \pm 0.4) \times 10^{-31}$ cm^6 molecule^{-2} s^{-1}, respectively. They also obtained $k_{1,\infty} = (1.5 \pm 0.3) \times 10^{-13}$ $(T/298\ \mathrm{K})^{(-1.3\pm0.3)}$ cm^3 molecule^{-1} s^{-1} over 298–363 K. The results for M = N_2 should be broadly similar to those for M = Ar while the high-pressure limit is of course independent of the nature of the bath gas. However, these rate constants are smaller than ours by factors of ~ 5 and ~ 100, respectively. They adjusted the adduct binding energy so as to match RRKM calculations to their experiments, and obtained 105 ± 8 kJ mol^{-1}. This value is significantly too high, by ca. 30 kJ mol^{-1} when compared to our high-level *ab initio* analysis.

We now speculate about possible chemistry at higher temperatures. Table 3 shows reaction enthalpies computed for 298 K via the CBS-QB3 method, and for reaction (2) analogs from experimental data [14, 31]. In $HOSO_2$, abstraction of H by O_2 is slightly exothermic and has a small activation energy of ~ 3 kJ mol^{-1} [15]. The analogous N–H bond in NH_2SO_2 is seen to be much stronger than the O–H

Table 3: Reaction enthalpies at 298 K.

reaction	CBS-QB3 $\Delta_r H_{298}$/ kJ mol^{-1}	reaction	Experimental[a] $\Delta_r H_{298}$/ kJ mol^{-1}
$NH_2SO_2 \rightarrow SO_2 + NH_2$	77	$HOSO_2 \rightarrow SO_2 + OH$	113
$NH_2SO_2 \rightarrow SO_2NH + H$	255	$HOSO_2 \rightarrow SO_3 + H$	195
$NH_2SO_2 + O_2 \rightarrow SO_2NH + HO_2$	49	$HOSO_2 + O_2 \rightarrow SO_3 + HO_2$	−11
$HNSO_2 \rightarrow SO_2 + NH$	213	$SO_3 \rightarrow SO_2 + O$	348

[a] refs [14, 31]

bond in $HOSO_2$, so that HO_2 formation by reaction with O_2 is 49 kJ mol^{-1} endothermic. We therefore expect an activation energy E_a comparable to or higher than the endothermicity which makes the abstraction by oxygen fairly slow. This effect is partly offset by the high $[O_2]$ expected in many combustion contexts. For a rough estimate we set E_a = 50 kJ mol^{-1} and use a pre-exponential factor A = 1×10^{-12} cm^3 molecule^{-1} s^{-1} chosen by analogy with O_2 + $HOSO_2$ [15]. At, say, 1000 K, these parameters imply a rate constant of $\sim 2 \times 10^{-15}$ cm^3 molecule^{-1} s^{-1} and, in 1 bar of air, a lifetime for NH_2SO_2 of 0.3 ms.

The product of such abstraction is $HNSO_2$. It may be seen to be less stable than the isoelectronic analog SO_3, with a S–N bond dissociation enthalpy 135 kJ mol^{-1} less than for S–O in SO_3. Thus dissociation of $HNSO_2$ is likely to be much faster than for SO_3. The CBS-QB3 value for the HN–SO_2 bond dissociation enthalpy at 298 K is 213 kJ mol^{-1}, which compares well with a CCSD(T)/CBS calculation by Méndez et al. that yielded 215 kJ mol^{-1} [32].

5 Conclusions

The present results extend the temperature range over which $NH_2 + SO_2$ has been studied, and suggest it is significantly faster than previously thought. The high-pressure limit is estimated from the removal rate of vibrationally excited NH_2. The results are consistent with an *ab initio* potential energy surface, which indicates that abstraction of H atoms from the adduct by O_2 is moderately endothermic, and that the resulting $HNSO_2$ species, isoelectronic with SO_3, could dissociate to NH + SO_2, leading to a cycle where NH_2 oxidation is catalyzed by SO_2.

Acknowledgement: PM thanks the Robert A. Welch Foundation (Grant B-1174) and the National Science Foundation (Grant CBET-0756144) for support. Computational facilities were purchased in part with NSF Grant CHE-0741936.

References

1. P. Glarborg, P. Combust. Inst. **31** (2007) 77.
2. A. Levy, P. Combust. Inst. **19** (1982) 1223.
3. J. O. L. Wendt, J. T. Morcomb, and T. L. Corley, P. Combust. Inst. **17** (1979) 671.
4. S. I. Tseregounis and O. I. Smith, Combust. Sci. Technol. **30** (1983) 231.
5. S. I. Tseregounis and O. I. Smith, 20th Symp. (Int.) Combust. (1984) 761.
6. T. L. Corley and J. O. L. Wendt, Combust. Flame **58** (1984) 141.
7. K. J. Hughes, A. S. Tomlin, V. A. Dupont, and M. Pourkashanian, Faraday Discuss. **119** (2001) 337.
8. P. Glarborg, A. D. Jensen, and J. E. Johnsson, Prog. Energ. Combust. **29** (2003) 89.
9. J. A. Silver, Combust. Flame **53** (1983) 17.
10. M. Oliva, M. U. Alzueta, J. C. Ibanez, A. Millera, and R. Bilbao, Proceedings of the 5th International Conference on Combustion Technologies for a Clean Environment, vol. II, Lisbon (1999), p. 867.
11. D. Lucas, N. J. Brown, Combust. Flame **49** (1983) 283.
12. P. Dagaut and A. Nicolle, P. Combust. Inst. **30** (2005) 1211.
13. A. A. Ioffe, V. P. Bulatov, V. A. Lozovsky, M. Y. Goldenberg, O. M. Sarkisov, and S. Y. Umansky, Chem. Phys. Lett. **156** (1989) 425.
14. M. A. Blitz, K. J. Hughes, and M. J. Pilling, J. Phys. Chem. A **107** (2003) 1971.
15. J. F. Gleason and C. J. Howard, J. Phys. Chem. **92** (1988) 3414.
16. G. Hennig, M. Klatt, B. Spindler, and H. G. Wagner, Ber. Bunsen. Phys. Chem. **99** (1995) 651.
17. Y. Gao and P. Marshall, Chem. Phys. Lett. **594** (2014) 30.
18. Y. Gao, I. M. Alecu, A. Goumri, and P. Marshall, Chem. Phys. Lett. **624** (2015) 83.
19. J. Naidoo, A. Goumri, and P. Marshall, P. Combust. Inst. **30** (2005) 1219.
20. H. Keller-Rudek, G. K. Moortgat, R. Sander, and R. Sörensen, The MPI-Mainz UV/VIS Spectral Atlas of Gaseous Molecules of Atmospheric Interest, www.uv-vis-spectral-atlas--mainz.org.
21. K. Luther and J. Troe, Influence of Temperature on Unimolecular and Termolecular Reactions, in: *Reactions of Small Transient Species*, A. Fontijn, M. A. A. Clyne (Eds.), Academic Press, London (1983), Ch. 2.
22. P. H. Wine, R. J. Thompson, A. R. Ravishankara, D. H. Semmes, C. A. Gump, A. Torabi, and J. M. Nicovich, J. Phys. Chem. **88** (1984) 2095.
23. M. J. Frisch, G. W. Trucks, H. B. Schlegel, G. E. Scuseria, M. A. Robb, J. R. Cheeseman, G. Scalmani, V. Barone, B. Mennucci, G. A. Petersson, H. Nakatsuji, M. Caricato, X. Li, H. P. Hratchian, A. F. Izmaylov, J. Bloino, G. Zheng, J. L. Sonnenberg, M. Hada, M. Ehara, K. Toyota, R. Fukuda, J. Hasegawa, M. Ishida, T. Nakajima, Y. Honda, O. Kitao, H. Nakai, T. Vreven, J. Montgomery, J. A., J. E. Peralta, F. Ogliaro, M. Bearpark, J. J. Heyd, E. Brothers, K. N. Kudin, V. N. Staroverov, R. Kobayashi, J. Normand, K. Raghavachari, A. Rendell, J. C.

Burant, S. S. Iyengar, J. Tomasi, M. Cossi, M. Rega, N. J., M. Klene, J. E. Knox, J. B. Cross, V. Bakken, C. Adamo, J. Jaramillo, R. E. Gomperts, O. Stratmann, A. J. Yazyev, R. Austin, C. Cammi, J. W. Pomelli, R. Ochterski, R. L. Martin, K. Morokuma, V. G. Zakrzewski, G. A. Voth, P. Salvador, J. J. Dannenberg, S. Dapprich, A. D. Daniels, O. Farkas, J. B. Foresman, J. V. Ortiz, J. Cioslowski, D. J. Fox, Gaussian 09, Gaussian, Wallingford, CT (2013).

24. J. A. Montgomery Jr., M. J. Frisch, J. W. Ochterski, and G. A. Petersson, J. Chem. Phys. **110** (1999) 2822.
25. H.-J. Werner, P. J. Knowles, R. Lindh, F. R. Manby, M. Schütz, P. Celani, T. Korona, A. Mitrushenkov, G. Rauhut, T. B. Adler, R. D. Amos, A. Bernhardsson, A. Berning, D. L. Cooper, M. J. O. Deegan, A. J. Dobbyn, F. Eckert, E. Goll, C. Hampel, G. Hetzer, T. Hrenar, G. Knizia, C. Köppl, Y. Liu, A. W. Lloyd, R. A. Mata, A. J. May, S. J. McNicholas, W. Meyer, M. E. Mura, A. Nicklaß, P. Palmieri, K. Pflüger, R. Pitzer, M. Reiher, U. Schumann, H. Stoll, A. J. Stone, R. Tarroni, T. Thorsteinsson, M. Wang, A. Wolf, *MOLPRO*, version 2010.1, a package of ab initio programs, 2010.
26. J. R. Barker, N. F. Ortiz, J. M. Preses, L. L. Lohr, A. Maranzana, P. J. Stimac, L. T. Nguyen, and T. J. D. Kumar, MultiWell-2011.1, University of Michigan, Ann Arbor, MI (2011), http://aoss-research.engin.umich.edu/multiwell/.
27. J. R. Barker, L. M. Yoder, and K. D. King, J. Phys. Chem. **105** (2001) 796.
28. J. Troe, J. Chem. Phys. **66** (1977) 4758.
29. D. C. McCabe, S. S. Brown, M. K. Gilles, R. K. Talukdar, I. W. M. Smith, and A. R. Ravishankara, J. Phys. Chem. A **107** (2003) 7762.
30. K. W. McKee, M. A. Blitz, P. A. Cleary, D. R. Glowacki, M. J. Pilling, P. W. Seakins, and L. Wang, J. Phys. Chem. A **111** (2007) 4043.
31. NIST Computational Chemistry Comparison and Benchmark Database, release 16a, http://cccbdb.nist.gov, R. D. Johnson III (Ed.), 2013.
32. M. Méndez, J. S. Francisco, and D. A. Dixon, Chem. Eur. J. **20** (2014) 10231.

Supplementary material: The online version of this article (DOI: 10.1515/zpch-2015-0637) provides supplementary material for authorized users.